

Modeling and Coverage Analysis for RIS-aided NOMA Transmissions in Heterogeneous Networks

Ziyi Xie, *Student Member, IEEE*, Wenqiang Yi, *Member, IEEE*,

Xuanli Wu, *Member, IEEE*, Yuanwei Liu, *Senior Member, IEEE*, and

Arumugam Nallanathan, *Fellow, IEEE*

Abstract

Reconfigurable intelligent surface (RIS) has been regarded as a promising tool to strengthen the quality of signal transmissions in non-orthogonal multiple access (NOMA) networks. This article introduces a heterogeneous network (HetNet) structure into RIS-aided NOMA multi-cell networks. A practical user equipment (UE) association scheme for maximizing the average received power is adopted. To evaluate system performance, we provide a stochastic geometry based analytical framework, where the locations of RISs, base stations (BSs), and UEs are modeled as homogeneous Poisson point processes (PPPs). Based on this framework, we first derive the closed-form probability density function (PDF) to characterize the distribution of the reflective links created by RISs. Then, both the exact expressions and upper/lower bounds of UE association probability are calculated. Lastly, the analytical expressions of the signal-to-interference-plus-noise-ratio (SINR) and rate coverage probability are deduced. Additionally, to investigate the impact of RISs on system coverage, the asymptotic expressions of two coverage probabilities are derived. The theoretical results show that RIS length is not the decisive factor for coverage improvement. Numerical results demonstrate that the proposed RIS HetNet structure brings significant enhancement in rate coverage. Moreover, there exists an optimal combination of RISs and BSs deployment densities to maximize coverage probability.

Index Terms

Heterogeneous network, non-orthogonal multiple access, reconfigurable intelligent surface, stochastic geometry, user association

I. INTRODUCTION

To enhance energy efficiency and network throughput, the controllable wireless communication environment becomes a new requirement for future networks. Reconfigurable intelligent

Z. Xie and X. Wu are with the School of Electronics and Information Engineering, Harbin Institute of Technology, Harbin 150001, China (email: {ziyi.xie, xlwu2002}@hit.edu.cn).

W. Yi, Y. Liu, and A. Nallanathan are with the School of Electronic Engineering and Computer Science, Queen Mary University of London, E1 4NS, U.K. (email: {w.yi, yuanwei.liu, a.nallanathan}@qmul.ac.uk).

Part of this work was submitted to IEEE Global Communications Conference (GLOBECOM), 2021 [1].

surface (RIS), also called intelligent reflecting surface (IRS), has been envisioned as a promising tool for providing this ability [2]–[4]. Specifically, RIS uses metamaterial or patch-array based technologies to alter the amplitude and/or phase of signals reflected by it [2], [5]. Compared with conventional active relays and small base stations (BSs), RISs are nearly passive and the energy is mainly consumed during the control and programming phase [6]. Based on the capability of smartly manipulating signal propagation, there are a variety of potential applications of RISs. One promising application is that RISs can be deployed to create strong line-of-sight (LoS) reflective links for blocked user equipment (UE). This coverage enhancement is of great significance for wireless networks, especially those with higher frequency bands such as millimeter wave and terahertz system, whose communication is vulnerable to blockages [7], [8].

For further enhancing the spectral efficiency of RIS-aided wireless networks, non-orthogonal multiple access (NOMA) has been considered to be an efficient booster as it is able to exploit the power domain to allocate the same resource block to multiple UEs [9]–[11]. Leveraging the difference of channel conditions among UEs, NOMA obtains the channel capacity gain over traditional orthogonal multiple access (OMA) schemes when considering UE fairness [12]. NOMA systems also benefit from the deployment of RISs. For NOMA UEs with weak channel gains, RISs are capable of creating stronger transmission paths. Moreover, since RISs are able to change the channel conditions of UEs, RISs offer a flexible decoding order for NOMA with different QoS requirements [13].

A. Related Works

For RIS-enabled communications, recent works have paid significant attention to system designs and performance analysis. As mentioned previously, RISs can be applied in various scenarios due to their nature of creating reflective paths. In [14], a three dimensional (3D) indoor communication model was considered and several RISs coated on walls were used to assist signal transmissions whose direct links are blocked. Regarding outdoor models, an IRS was located at a cell edge to improve the communication quality of a nearby UE in [15]. In [16], a holographic RIS was deployed to provide passive beamforming between the servig BS and UEs under terahertz systems. The authors in [17] employed IRSs for air-ground networks to control the reflection direction of radio waves and hence the inter-cell interference can be suppressed. These works are under the assumption that the locations of RISs are known and

the transmission paths are predefined. To characterize the random locations of RISs in large-scale deployment networks, stochastic geometry is an efficient mathematical tool. A recent work [18] focused on spatial throughput in a multi-user single-cell network, where IRSs are randomly deployed in a ring area. Average performance for multi-cell networks was evaluated in some research articles, such as [8], [19], [20], while the complex reflective channels impose challenges on UE association and subsequent analysis. In [8], the authors studied a special case that UEs in blind-spot areas obtain indirect LoS links through RISs coated blockages. For tractability, the authors in [19] proposed a two-step association strategy in a millimeter wave multi-antenna system. Based on this strategy, the enhancement of capacity and energy efficiency is validated. In [20], UEs associated to their nearest BSs and the corresponding communication was also assisted by IRSs. This work showed that the composite channel gain can be approximated by the Gamma distribution.

Sparked by the aforementioned potential benefits of integrating RISs and NOMA, the majority of research efforts have been devoted to RIS-NOMA networks. In [21], the authors proposed a design that an IRS was deployed to assist the transmission from a BS to cell-edge NOMA users while cell-center NOMA users associated to the BS directly. The authors in [22] focused on the dead zone users and jointly optimized the beamforming vectors at BSs and IRSs. The above RIS-aided paradigms assumed that there is no direct links between users and BSs. In practice, BS-UE links always exist although the channel gain may be degraded by blockages, so in [23]–[25], both BS-UE links and BS-RIS-UE links were considered. In [23], the authors assumed all RIS-related channels are LoS while BS-user channels are non-line-of-sight (NLoS), and presented an optimization framework to minimize the total transmit power. Two insightful works, [24] and [25], solved the joint optimization problem over multiple factors including RIS parameters, subchannel assignment, and decoding order for maximizing system sum rates. Furthermore, some works have contributed to the analysis of theoretical performance in RIS-NOMA networks. The authors in [26] compared the outage probability and ergodic rate between NOMA and OMA in IRS-enabled communications and validated the enhancement from IRS-NOMA schemes. The authors in [27] evaluated the network performance by deriving the best-case and worst-case of channel statistics. Stochastic geometry models were considered in [13], [27], [28]. The authors in [27] and [28] modeled the locations of users as a homogeneous Poisson point processes (PPPs) and studied the spatial effect in single-cell networks. The authors in [13] introduced a tractable path loss model for large-scale deployment of RISs and extended the RIS-aided model

to multi-cell scenarios.

B. Motivations and Contributions

As discussed in the previous section, RIS is an efficient solution for the performance enhancement of NOMA systems. Although the BS-RIS-UE link significantly strengthens the quality of signal transmissions, most existing works assumed the direct links between BS and UE are weak or blocked but neglected the probability of LoS direct links. In these works, signal transmissions were always assisted by RISs hence UE association schemes were scarcely investigated. Furthermore, due to the complexity of the reflective paths provided by RISs, the research on theoretical performance in multi-cell scenarios is still insufficient.

Motivated by these three reasons, in this paper, we introduce a heterogeneous network (HetNet) structure into RIS-aided NOMA multi-cell networks. A UE association scheme is provided according to channel conditions. Considering the deployment of devices in large-scale RIS-NOMA networks, we use stochastic geometry for system modeling and performance evaluation. The main contributions are summarized as follows:

- We provide an analytical framework for the downlink NOMA RIS HetNets based on stochastic geometry. In this framework, We model the random locations of RISs, BSs, and UEs by independent homogeneous PPPs. To maximize channel gains for signal transmissions, we employ a practical UE association rule in which UEs associate either a BS or RIS with higher average received power, where correlated RIS channels are considered. Moreover, we consider LoS/NLoS transmissions for the direct BS-UE links and LoS transmissions for the BS-RIS-UE links to depict a general scenario.
- We characterize the distance distribution of BS-RIS-UE links and derive its closed-form probability density function (PDF). Based on general path models for BS-UE links and BS-RIS-UE links, we derive the UE association probability of a typical UE in paired NOMA UEs. We also provide the bounds of the UE association probability and show the impact of LoS probability.
- We derive the analytical expressions for the signal-to-interference-plus-noise-ratio (SINR) and rate coverage probability of the typical NOMA UE. To investigate the impact of RISs, we deduce the closed-form asymptotic expressions of these two performance metrics versus the half-length of RISs L . The theoretical results indicate that we cannot obtain the maximum

achievable performance only by enlarging the length of RISs. Additionally, a tractable approximation is calculated for the rate coverage.

- The simulation results validate our theoretical analysis and show that 1) compared with OMA or non-RIS scenarios, the proposed NOMA HetNet structure enhances the coverage probability and thus improving the spectral efficiency; 2) the densification of BSs enhances signal transmissions for both BS-UE links and BS-RIS-UE links; 3) there exists an optimal RIS length to maximize the system performance; 4) when the density of BSs is predefined, we can choose an optimal RISs deployment density to maximize the system performance.

C. Organizations and Notations

The remainder of this paper is organized as follows. In section II, we describe the system model of NOMA RIS HetNets. In section III, we present the path loss models including angle and distance distributions. Additionally, we derive the association probability for each tier. In section IV, we derive the analytical expressions of SINR and rate coverage probability. In section V, we illustrate numerical results. In section VI, we propose our conclusion. Notations in this paper are listed in Table I.

TABLE I
TABLE OF NOTATIONS

Notation	Description
$\Phi_B; \Phi_R; \Phi_U$	PPP of BSs; PPP of RISs; PPP of UEs
$\lambda_B; \lambda_R; \lambda_U$	Density of BSs; density of RISs; density of UEs
$\tilde{\Phi}_B; \tilde{\lambda}_B$	PPP of active BSs; density of active BSs
$P_B; W$	Transmit power of BSs; system bandwidth
$C_\kappa; C_R$	Intercept of BS-UE links ($\kappa \in \{L, N\}$); intercept of BS-RIS-UE links
$\alpha_\kappa; \alpha_R$	Path loss exponent of BS-UE links ($\kappa \in \{L, N\}$); path loss exponent of BS-RIS-UE links
$m_\kappa; m_R$	Nakagami coefficient of BS-UE links ($\kappa \in \{L, N\}$); Nakagami coefficient of BS-RIS-UE links
$\theta_{BR}; \theta_{RU}; L$	Angle of arrival; angle of departure; half-length of RIS
$a_s; a_l$	Power allocation factor of small path loss UE; power allocation factor of large path loss UE
$\beta; \sigma^2$	Blockage parameter; thermal noise

II. SYSTEM MODEL

This work considers RIS-aided downlink NOMA networks with a HetNet structure, where BSs, RISs, and UEs are modeled as three independent homogeneous PPPs Φ_B , Φ_R , and Φ_U in \mathbb{R}^2 with density λ_B , λ_R , and λ_U , respectively. The transmit power of BSs is P_B and the system bandwidth is W . Since a BS is silent if there is no UE associated to it, the locations of active BSs also obeys PPP with density $\tilde{\lambda}_B = \lambda_B \left(1 - \left(1 + \frac{\lambda_U}{3.5\lambda_B}\right)^{-3.5}\right)$, [29]. Both BSs and UEs are equipped with a single antenna. For RISs, we consider a linear model with $2L$ in length [30]. According to NOMA principles, two NOMA UEs are grouped in each resource block (RB) to improve the spectral efficiency. For simplicity, we assume that one of the paired UEs has been associated to a BS in the previous UE association process, and hence its communication distance d_C is known at the serving BS. A typical UE is randomly selected from Φ_U , which joins the same RB of one connected user to form a NOMA group. The location of this typical UE is fixed at the origin of the considered plane.

A. Channel Model

In this RIS HetNet, there are two types of communication links between BSs and UEs: 1) BS-UE link, the link that a BS transmit signals directly to its served UEs; 2) BS-RIS-UE link, the link that an assisted RIS is used to reflect signals from a BS to its UEs. In the former case, we adopt a stochastic blockage model for LoS/NLoS propagation [31]. The blockages are modeled as a rectangle Boolean scheme and the LoS transmission probability between BSs and UEs is shown as

$$p_L(d_0) = e^{-\beta d_0}, \quad (1)$$

where β is a parameter determined by the density and the average size of the blockages.

For the BS-UE links, the path loss can be expressed as

$$L_{BU}(d_0) = \sum_{\kappa \in \{L, N\}} \mathbb{B}(p_\kappa(d_0)) L_{BU, \kappa}(d_0), \quad (2)$$

with

$$L_{BU, \kappa}(d_0) = C_\kappa d_0^{-\alpha_\kappa}, \quad (3)$$

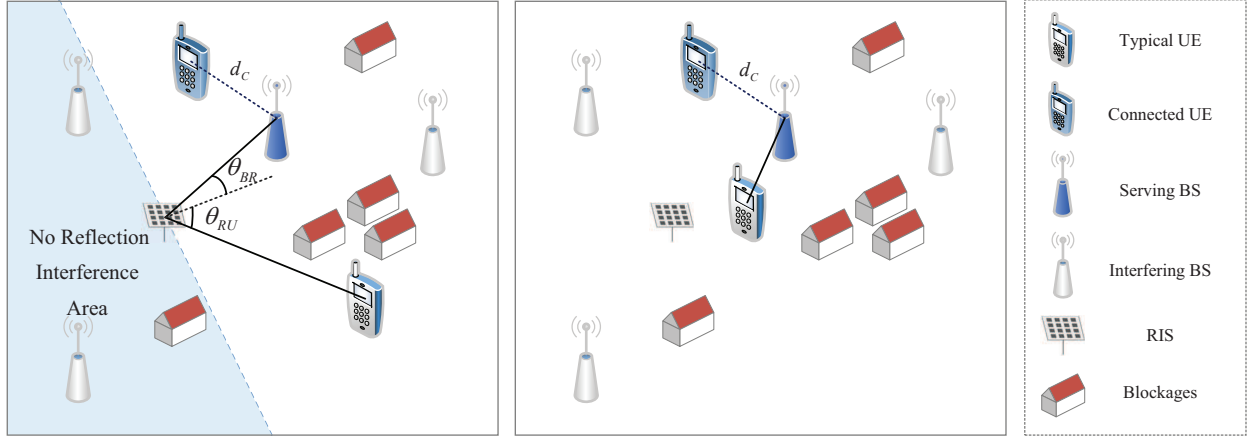


Fig. 1. Illustration of the UE association model: (a) Left: The typical UE associates to BS through BS-RIS-UE link; (b) Right: The typical UE associates to BS through BS-UE link.

where C_κ is the path loss at a reference distance $d_0 = 1$ and α_κ denotes the path loss exponent. The $\kappa = L$ and $\kappa = N$ represent LoS and NLoS links, respectively. The probability for NLoS transmissions is $p_N(d_0) = 1 - p_L(d_0)$. $\mathbb{B}(t)$ is a Bernoulli random variable with a probability of success t .

For the BS-RIS-UE links, the angle of arrival at a RIS is denoted by θ_{BR} and the angle of departure is denoted by θ_{RU} . According to [13], the path loss under correlated channels can be expressed as

$$L_{RIS}(d_{BR}, d_{RU}) = C_R(d_{BR}d_{RU})^{-\alpha_R}, \quad (4)$$

where d_{BR} denotes the distance between BS and RIS. The d_{RU} is the distance between RIS and the typical UE. The intercept is denoted by $C_R = \frac{L^2}{16\pi^2} (\cos(\theta_{BR}) + \cos(\theta_{RU}))^2$. The α_R is the path loss exponent. It should be noted that the BS-RIS-UE links exist only when the BSs and the UEs are distributed at the same side of the RIS.

B. UE Association in RIS HetNets

For the UE association, we assume that the typical UE connects to the BS or RIS with the highest received power. In other words, the typical UE associates to the nearest LoS BS or associates to the nearest RIS which reflects signals from its nearest BS. Let Φ_U^L and Φ_U^R denote the set of UEs associated to LoS BSs and the set of UEs associated to BSs with the aid of RISs, respectively. Therefore, we have $\Phi_U^L \cup \Phi_U^R = \Phi_U$.

If the typical UE $u_0 \in \Phi_U^L$ associates to the BS $j \in \Phi_B$, the average received power of the desired signal at the typical UE can be expressed as

$$P_{0,j} = a_t P_B L_{BU,L}(d_{0,j}), \quad (5)$$

where $d_{0,j}$ is the distance between the typical UE and its nearest LoS BS. The a_t is the power allocation factor for the typical UE.

On the other hand, if the typical UE $u_0 \in \Phi_U^R$ associates to the BS $j \in \Phi_B$ through the RIS $i \in \Phi_R$, the average received power of the desired signal at the typical UE can be expressed as

$$P_{0,j}^{(i)} = a_t P_B L_{RIS}(d_{BR,j}^{(i)}, d_{RU,0}^{(i)}), \quad (6)$$

where $d_{BR,j}^{(i)}$ is the distance between the serving BS and the assistant RIS. The $d_{RU,0}^{(i)}$ is the distance between the assistant RIS and the typical UE.

For the connected UE, it associates to the BS through BS-UE link, so the average received power of the desired signal at the connected UE can be expressed as

$$P_C = a_c P_B L_{BU,L}(d_C). \quad (7)$$

where a_c is the power allocation factor for the connected UE.

C. SINR Analysis

Since the average performance of wireless communications mainly depends on the path loss, we assume the successive interference cancelation (SIC) in a NOMA group is processed at the UE with the smaller path loss. As it is not pre-determined whether the path loss of the typical UE is large or small, we have the following two cases.

1) *Small Path Loss Case*: When the typical UE has the smaller path loss than the connected UE, the typical UE first decodes the information of the connected UE associated to the same BS. For power allocation, a_l and a_s are the power allocation factors for large path loss UE and small path loss UE, respectively. The power allocation factors also satisfy the conditions that $a_s \leq a_l$ and $a_l + a_s = 1$. Thus, in this case, $a_t = a_s$ and $a_c = a_l$. For simplicity, we denote $\tilde{c}_{LR} = \frac{C_L}{C_R}$, $\tilde{c}_{RL} = \frac{C_R}{C_L}$, $\tilde{\alpha}_{LR} = \frac{\alpha_L}{\alpha_R}$ and $\tilde{\alpha}_{RL} = \frac{\alpha_R}{\alpha_L}$ in the following parts of this work.

If the typical UE $u_0 \in \Phi_U^L$, $d_{0,j} \leq d_C$ holds and the SINR for the SIC process at u_0 is given

by

$$\gamma_{t \rightarrow c, small}^L = \frac{a_l P_B L_{BU,L}(d_{0,j}) h_{0,j}^{L^2}}{a_s P_B L_{BU,L}(d_{0,j}) h_{0,j}^{L^2} + I_L + I_N + \sigma^2}, \quad (8)$$

where $I_L = \sum_{k \in \Phi_B^L \setminus j} P_B L_{BU,L}(d_{0,k}) h_{0,k}^{L^2}$ is the interference from other LoS BSs. The $I_N = \sum_{k \in \Phi_B^N} P_B L_{BU,N}(d_{0,k}) h_{0,k}^{N^2}$ is the interference from NLoS BSs. For $\kappa = \{L, N\}$, $h_{0,k}^{\kappa^2}$ is the small scale fading power from the BS $k \in \Phi_B$. We characterize the small scale fading as Nakagami- m distribution with an integer parameter m_κ . Moreover, σ^2 is the additive white Gaussian noise power.

After the SIC process, the decoding SINR at the typical UE u_0 can be expressed as

$$\gamma_{t, small}^L = \frac{a_s P_B L_{BU,L}(d_{0,j}) h_{0,j}^{L^2}}{I_L + I_N + \sigma^2}. \quad (9)$$

We denote $d_{0,j}^{(i)} = d_{BR,j}^{(i)} d_{RU,0}^{(i)}$. If the typical UE $u_0 \in \Phi_U^R$, i.e. $d_{0,j}^{(i)} \leq (\tilde{c}_{RL})^{\frac{1}{\alpha_R}} d_C^{\tilde{\alpha}_{LR}}$, the SINR for the SIC process at u_0 is given by

$$\gamma_{t \rightarrow c, small}^R = \frac{a_l P_B L_{RIS}(d_{BR,j}^{(i)}, d_{RU,0}^{(i)}) h_{0,j}^{(i)^2}}{a_s P_B L_{RIS}(d_{BR,j}^{(i)}, d_{RU,0}^{(i)}) h_{0,j}^{(i)^2} + I_R + I_L + I_N + \sigma^2}, \quad (10)$$

where $I_R = \sum_{k \in \Phi_B^R \setminus j} P_B L_{RIS}(d_{BR,k}^{(i)}, d_{RU,0}^{(i)}) h_{0,k}^{(i)^2}$ is the interference from BSs located at the same side of serving RIS i . We assume that only the serving RIS is pointed at the typical UE, so the links between the other RISs and the typical UE are blocked. The $h_{0,k}^{(i)^2}$ is the small scale fading power from the BS $k \in \Phi_B$, which also follows Nakagami- m distribution with an integer parameter m_R .

Thus, the decoding SINR at the typical UE u_0 can be expressed as

$$\gamma_{t, small}^R = \frac{a_s P_B L_{RIS}(d_{BR,j}^{(i)}, d_{RU,0}^{(i)}) h_{0,j}^{(i)^2}}{I_R + I_L + I_N + \sigma^2}. \quad (11)$$

2) *Large Path Loss Case*: When the typical UE has larger path loss, the SIC process occurs at the connected UE, while the signal transmitted to the connected UE is regarded as interference at the typical UE. In this case, $a_t = a_l$ and $a_c = a_s$.

If the typical UE $u_0 \in \Phi_U^L$, i.e. $d_{0,j} > d_C$, the decoding SINR for u_0 is as follows

$$\gamma_{t, large}^L = \frac{a_l P_B L_{BU,L}(d_{0,j}) h_{0,j}^{L^2}}{a_s P_B L_{BU,L}(d_{0,j}) h_{0,j}^{L^2} + I_L + I_N + \sigma^2}. \quad (12)$$

On the other hand, If the typical UE $u_0 \in \Phi_U^R$, i.e. $d_{0,j}^{(i)} > (\tilde{c}_{RL})^{\frac{1}{\alpha_R}} d_C^{\tilde{\alpha}_{LR}}$, the decoding SINR for u_0 can be expressed as

$$\gamma_{t,large}^R = \frac{a_l P_B L_{RIS}(d_{BR,j}^{(i)}, d_{RU,0}^{(i)}) h_{0,j}^{(i)2}}{a_s P_B L_{RIS}(d_{BR,j}^{(i)}, d_{RU,0}^{(i)}) h_{0,j}^{(i)2} + I_R + I_L + I_N + \sigma^2}. \quad (13)$$

For the connected UE, since its location and the association choice are known, the expression of SINR is much simpler than that for typical UE. As the performance of the connected UE has been investigated in [13], we only focus on the typical UE in this work.

III. PATH LOSS AND ASSOCIATION ANALYSIS IN RIS HETNETS

In this section, we first derive the expressions of some relevant distance distributions, based on which the UE association probability is investigated. Then, we provide the angle distributions for RIS-aided links, which are also fundamental for subsequent coverage performance analysis.

A. Distance Distributions of the Nearest BS

For the typical UE $u_0 \in \Phi_U$, BSs in the system can be divided into two independent sets: LoS BSs Φ_B^L and NLoS BSs Φ_B^N . According to the ‘‘Thinning Theorem’’ [32, Theorem 2.36], the locations of LoS BSs and NLoS BSs obey inhomogeneous PPPs of density $\lambda_B^L(d_0) = \lambda_B p_L(d_0)$ and $\lambda_B^N(d_0) = \lambda_B p_N(d_0)$ at distance d_0 , respectively. As the typical UE can associate to a LoS BS when at least one LoS transmission link exists, the following lemma first provides the probability that the set Φ_B^L is non-empty.

Lemma 1. *The probability that the typical UE has at least one LoS BS is as follows*

$$P_L = 1 - \exp\left(-\frac{2\pi\lambda_B}{\beta^2}\right). \quad (14)$$

Proof: Based on [33, Theorem 8], the probability P_L can be expressed as $P_L = 1 - \lim_{x \rightarrow \infty} \mathbb{P}(d_{0,j} > x) = 1 - \exp\left(-2\pi \int_0^\infty r \lambda_B^L(r) dr\right)$. By plugging (1), (14) is obtained. ■

Thus, the probability that all LoS links are blocked for the typical UE is $P_N = 1 - P_L = \exp\left(-\frac{2\pi\lambda_B}{\beta^2}\right)$. Then, the distribution of the distance to the nearest BS in Φ_B^L is calculated as below.

Lemma 2. For BS-UE links, the PDF of the distance between the typical UE and its nearest LoS BS $d_{0,j}$ can be given by

$$f_{d_{0,j}}(x) = 2\pi\lambda_B x p_L(x) \exp\left(-2\pi\lambda_B \int_0^x r p_L(r) dr\right). \quad (15)$$

Proof: Using the feature of the inhomogeneous PPP Φ_B^L , the cumulative distribution function (CDF) of $d_{0,j}$ is given by

$$F_{d_{0,j}}(x) = 1 - \exp\left(-2\pi\lambda_B \int_0^x r p_L(r) dr\right). \quad (16)$$

The PDF of $d_{0,j}$ can be calculated by $f_{d_{0,j}}(x) = \frac{d}{dx} F_{d_{0,j}}(x)$. Thus, the PDF is obtained as (15). ■

Noticed that the locations of UEs, RISs, and BSs follow independent homogeneous PPPs, the PDF of the distance between a RIS and its nearest BS $d_{BR,j}^{(i)}$ as well as the PDF of the distance between the typical UE and its nearest RIS $d_{RU,0}^{(i)}$ can be given by

$$f_{d_{BR}}(x) = 2\pi\lambda_B x \exp(-\pi\lambda_B x^2), \quad (17)$$

$$f_{d_{RU}}(x) = 2\pi\lambda_R x \exp(-\pi\lambda_R x^2). \quad (18)$$

Lemma 3. For BS-RIS-UE links, the PDF of the distance between the typical UE and its nearest BS $d_{0,j}^{(i)}$ can be given by

$$f_{d_{0,j}^{(i)}}(x) = 4\pi^2 x \lambda_B \lambda_R K_0\left(2\pi x \sqrt{\lambda_B \lambda_R}\right), \quad (19)$$

where $K_0(\cdot)$ is modified Bessel function of the second kind [34, eq. (8.447.3)].

Proof: See Appendix A. ■

B. UE Association Probability

As mentioned in II-B, the typical UE chooses the communication link with maximum average received power. The following Theorem provides the UE probability for each tier in this RIS HetNets.

Theorem 1. *The probability that the typical UE associates to a LoS BS, defined as $A_L = \mathbb{P}(u_0 \in \Phi_U^L)$, can be calculated as*

$$A_L = 4\pi^2 \lambda_B \lambda_R \int_0^\infty x \left(1 - \exp \left(-2\pi \lambda_B \int_0^{\varphi(x)} r p_L(r) dr \right) \right) K_0 \left(2\pi x \sqrt{\lambda_B \lambda_R} \right) dx, \quad (20)$$

where $\varphi(x) = (\tilde{c}_{LR})^{\frac{1}{\alpha_L}} x^{\tilde{\alpha}_{RL}}$. Thus, the probability that the typical UE connects to a RIS is $A_R = \mathbb{P}(u_0 \in \Phi_U^R) = 1 - A_L$.

Proof: When the typical UE obtains larger received power from a LoS BS rather than a RIS, i.e. $P_{0,j} > P_{0,j}^{(i)}$, the typical UE associates to a LoS BS through BS-UE link. Therefore,

$$\begin{aligned} A_L &= \mathbb{P} \left(a_t P_B C_L d_{0,j}^{-\alpha_L} \geq a_t P_B C_R d_{BU,j}^{(i) -\alpha_R} \right) \\ &= \mathbb{P} \left(d_{0,j} \leq (\tilde{c}_{LR})^{\frac{1}{\alpha_L}} d_{0,j}^{(i) \tilde{\alpha}_{RL}} \right) \\ &= \int_0^\infty \mathbb{P} \left(d_{0,j} \leq (\tilde{c}_{LR})^{\frac{1}{\alpha_L}} x^{\tilde{\alpha}_{RL}} \right) f_{d_{0,j}^{(i)}}(x) dx. \end{aligned} \quad (21)$$

Based on (16) and (19), the results in (20) can be obtained. ■

Remark 1. *When $x < \infty$, $\varphi(x) < \infty$ always holds. The upper bound of A_L can be calculated as*

$$\begin{aligned} A_L &< 4\pi^2 \lambda_B \lambda_R \int_0^\infty x \left(1 - \exp \left(-2\pi \lambda_B \int_0^\infty r p_L(r) dr \right) \right) K_0 \left(2\pi x \sqrt{\lambda_B \lambda_R} \right) dx \\ &= 4\pi^2 \lambda_B \lambda_R \int_0^\infty x P_L K_0 \left(2\pi x \sqrt{\lambda_B \lambda_R} \right) dx \\ &= P_L. \end{aligned} \quad (22)$$

Thus, the lower bound of A_R is P_N . It can be explained that the UEs associate to BSs through BS-RIS-UE links when all LoS BS-UE links are blocked. According to (14), in the sparse BS or dense blockage environment, the probability that a UE is blocked is high, so most UEs acquire signal from RISs for larger received power.

Corollary 1. *For the special case that $p_L(x) = 1$ and $\alpha_L = 2\alpha_R$, the UE association probability for $u_0 \in \Phi_U^L$ can be expressed in closed form as*

$$A_L = 1 - \frac{4\tilde{\lambda}_{RB}}{c_{LR}^4 - 4\tilde{\lambda}_{RB}} \left(\frac{c_{LR}^2}{\sqrt{c_{LR}^4 - 4\tilde{\lambda}_{RB}}} \ln \left(\frac{c_{LR}^2}{2\sqrt{\tilde{\lambda}_{RB}}} + \sqrt{\frac{c_{LR}^4}{4\tilde{\lambda}_{RB}} - 1} \right) - 1 \right), \quad (23)$$

where $c_{LR} = (\tilde{c}_{LR})^{\frac{1}{\alpha_L}}$ and $\tilde{\lambda}_{RB} = \lambda_R/\lambda_B$.

Proof: In this case, $\varphi(x) = (\tilde{c}_{LR})^{\frac{1}{\alpha_L}} x^{\frac{1}{2}}$ and (20) can be rewritten as

$$A_L = 4\pi^2 \lambda_B \lambda_R \int_0^\infty x \left(1 - \exp\left(-\pi \lambda_B (\tilde{c}_{LR})^{2/\alpha_L} x\right)\right) K_0\left(2\pi x \sqrt{\lambda_B \lambda_R}\right) dx. \quad (24)$$

By using eq. (6.561.16) and eq. (6.624.1) in [34], (23) is obtained. ■

Corollary 2. For the special case that $p_L(x) = 1$ and $\alpha_L = \alpha_R$, the UE association probability for $u_0 \in \Phi_U^L$ can be expressed in closed form as

$$A_L = 1 - \frac{\sqrt{\pi \lambda_R}}{c_{LR}} \exp\left(\frac{\pi \lambda_R}{2c_{LR}^2}\right) W_{-\frac{1}{2}, 0}\left(\frac{\pi \lambda_R}{c_{LR}^2}\right), \quad (25)$$

where $W_{\cdot, \cdot}(\cdot)$ is the Whittaker function [34, eq. (9.220.2)].

Proof: In this case, $\varphi(x) = (\tilde{c}_{LR})^{\frac{1}{\alpha_L}} x$. Using eq. (6.561.16) and eq. (6.631.3) in [34], this corollary is proved. ■

Remark 2. In these special cases, the value of P_L is related to $\tilde{\lambda}_{RB}$ or λ_R rather than the exact density of BSs λ_B . Thus, in these non-blockage environments, the received power at UEs can also be improved by deploying denser RISs.

C. Angle Distribution

As shown in (4), for the typical UE, the path loss expression of BS-RIS-UE link relates to the angle of arrival $\theta_{BR,0}$ and the angle of departure $\theta_{RU,0}$. Since the reflective surfaces are regarded as RISs rather than mirrors, $\theta_{BR,0}$ and $\theta_{RU,0}$ can be unequal.

According to [13, Remark 1], the angle $\theta = \theta_{BR,0} + \theta_{RU,0}$ is uniformly distributed in $[0, \pi]$. We denote $\varepsilon_0 \in (0, 1)$, so the angle of arrival and the angle of departure can be expressed as $\theta_{BR,0} = \varepsilon_0 \theta$ and $\theta_{RU,0} = (1 - \varepsilon_0) \theta$, respectively. The PDFs of the angle of arrival and departure are as follows

$$f_{\theta_{BR,0}}(x) = \frac{1}{\pi \varepsilon_0}, \quad x \in \left(0, \frac{\pi}{2}\right), \quad (26)$$

$$f_{\theta_{RU,0}}(x) = \frac{1}{\pi(1 - \varepsilon_0)}, \quad x \in \left(0, \frac{\pi}{2}\right). \quad (27)$$

As the angles of arrival and departure obey uniform distributions, C_R can be approximated as the average value

$$C_R \approx \mathbb{E}[C_R] = \frac{L^2}{16\pi^3} \left(\pi + \frac{\sin(2\varepsilon_0\pi)}{4\varepsilon_0 - 12\varepsilon_0^2 + 8\varepsilon_0^3} \right). \quad (28)$$

The intercept of the path loss for BS-RIS-UE links has a positive correlation with the length of RISs. Thus, we can use larger RISs to enhance the channel conditions.

IV. COVERAGE PROBABILITY ANALYSIS

The coverage probability is generally defined as the probability that the typical UE can successfully transmit signals with a targeted SINR τ_t or a targeted data rate ρ_t . In this section, we provide both the SINR coverage probability and rate coverage probability of the typical UE $u_0 \in \Phi_U$.

A. Laplace Transform of Interference

Before analyzing the coverage performance of this system, three kinds of Laplace transforms of interference are derived first. Only active BSs become the interfering BSs. Let $I_{total} = I_L + I_N + I_R$ denote the total interference to the typical UE, where I_L , I_N , and I_R are the interference from LoS BSs, NLoS BSs, and RISs, respectively. The Laplace transform of I_{total} is $\mathcal{L}_{I_{total}}(s) = \mathcal{L}_{I_L}(s)\mathcal{L}_{I_N}(s)\mathcal{L}_{I_R}(s)$.

1) *Interference from LoS BSs*: For both conditions that the typical UE associates to a LoS BS and the typical UE associates to a RIS, the Laplace transform of the interference from LoS BSs can be expressed as

$$\mathcal{L}_{I_L}(s) = \mathbb{E} \left[\exp \left(-s \sum_{k \in \Phi_B^L \setminus j} P_B L_{BU,L}(d_{0,k}) h_{0,k}^L \right) \right]. \quad (29)$$

Lemma 4. *The Laplace transform of the interference from LoS BSs is derived as*

$$\mathcal{L}_{I_L}(s) = \exp \left(-2\pi \tilde{\lambda}_B \int_{d_{0,min}}^{\infty} \left(1 - \left(1 + \frac{s P_B L_{BU,L}(x)}{m_L} \right)^{-m_L} \right) x p_L(x) dx \right), \quad (30)$$

where $d_{0,min} = \min \left\{ d_{0,j}, \varphi \left(d_{0,j}^{(i)} \right) \right\}$ is the minimum distance between the typical UE and interfering BSs.

Proof: See Appendix B. ■

2) *Interference from NLoS BSs*: Similarly, the Laplace transform of the interference from NLoS BSs can be expressed as

$$\mathcal{L}_{I_N}(s) = \mathbb{E} \left[\exp \left(-s \sum_{k \in \Phi_B^N \setminus j} P_B L_{BU,N}(d_{0,k}) h_{0,k}^N \right) \right]. \quad (31)$$

Lemma 5. *The Laplace transform of the interference from NLoS BSs is derived as*

$$\mathcal{L}_{I_N}(s) = \exp \left(-2\pi \tilde{\lambda}_B \int_0^\infty \left(1 - \left(1 + \frac{s P_B L_{BU,N}(x)}{m_N} \right)^{-m_N} \right) x p_N(x) dx \right). \quad (32)$$

Proof: Since the typical UE can not associate to a NLoS BS directly, the minimum distance between the typical UE and interfering NLoS BSs is 0. The derivation procedure is the same as the proof in **Lemma 4**. ■

3) *Interference from RISs*: If the typical UE associates to a BS through BS-RIS-UE link, it receives signal as well as interference reflected from the serving RIS. Under this condition, the Laplace transform of the interference from the RIS can be expressed as

$$\mathcal{L}_{I_R}(s) = \mathbb{E} \left[\exp \left(-s \sum_{k \in \Phi_B^R \setminus j} P_B L_{RIS}(d_{BR,k}^{(i)}, d_{RU,0}^{(i)}) h_{0,k}^R \right) \right]. \quad (33)$$

Lemma 6. *The Laplace transform of the interference from the assistant RIS is derived as*

$$\mathcal{L}_{I_R}(s) = \exp \left(-\delta_1 \left({}_2F_1 \left(m_R, -\frac{2}{\alpha_R}; 1 - \frac{2}{\alpha_R}; -s\delta_2 \right) - 1 \right) \right), \quad (34)$$

where $\delta_1 = \frac{\pi \tilde{\lambda}_B d_{BR,j}^{(i)2}}{2}$, $\delta_2 = \frac{P_B L_{RIS}(d_{BR,j}^{(i)}, d_{RU,0}^{(i)})}{m_R}$, and ${}_2F_1(\cdot, \cdot; \cdot; \cdot)$ is the Gauss hypergeometric function.

Proof: See Appendix C. ■

B. SINR Coverage Probability

Based on the distributions of the relevant distance $d_{0,j}$, $d_{BR,j}^{(i)}$, and $d_{RU,0}^{(i)}$, the association probabilities A_L , and the Laplace transforms of interference I_L , I_N , and I_R , we proceed to derive the analytical expression of the SINR coverage probability. According to the path losses, two cases are considered in the following.

1) *Small Path Loss Case:* In this case, the typical UE decodes its own message after a successful SIC process, and the SINR coverage probability is expressed as

$$P_{cov,small} = \mathbb{P}(\gamma_{t \rightarrow c,small} > \tau_c, \gamma_{t,small} > \tau_t), \quad (35)$$

where τ_c and τ_t are the targeted SINRs of the connected UE and the typical UE, respectively.

If the typical UE $u_0 \in \Phi_U^L$ and $a_l - \tau_c a_s > 0$, the SINR coverage probability can be rewritten as

$$P_{cov,small}^L(d_{0,j}) = \mathbb{P}\left(h_{0,j}^2 > \frac{\tau^*(I_L + I_N + \sigma^2)}{P_B L_{BU,L}(d_{0,j})}\right), \quad (36)$$

where $\tau^* = \max\left(\frac{\tau_c}{a_l - \tau_c a_s}, \frac{\tau_t}{a_s}\right)$.

Lemma 7. *If $a_l - \tau_c a_s > 0$ holds, the approximated SINR coverage probability of the typical UE $u_0 \in \Phi_U^L$ for the small path loss case is derived as*

$$P_{cov,small}^L(d_{0,j}) \approx \sum_{n=1}^{m_L} (-1)^{n+1} \binom{m_L}{n} \mathcal{L}_{I_L}(s_L) \mathcal{L}_{I_N}(s_L) e^{-s_L \sigma^2}, \quad (37)$$

where $s_L = \frac{n\eta_L \tau^*}{P_B L_{BU,L}(d_{0,j})}$ and $\eta_L = m_L (m_L!)^{-\frac{1}{m_L}}$. Otherwise, $P_{cov,small}^L(d_{0,j}) = 0$.

Proof: According to [35], the normalized Gamma variable h^2 with parameter m has a tight lower bound $\mathbb{P}(h^2 < x) > (1 - e^{-\eta x})^m$, where $\eta = m(m!)^{-\frac{1}{m}}$. Utilizing binomial expansions, (37) is obtained. ■

If the typical UE $u_0 \in \Phi_U^R$ and $a_l - \tau_c a_s > 0$, the SINR coverage probability can be rewritten as

$$P_{cov,small}^R(d_{BR,j}^{(i)}, d_{RU,0}^{(i)}) = \mathbb{P}\left(h_{0,j}^{(i)2} > \frac{\tau^*(I_R + I_L + I_N + \sigma^2)}{P_B L_{RIS}(d_{BR,j}^{(i)}, d_{RU,0}^{(i)})}\right). \quad (38)$$

Lemma 8. *If $a_l - \tau_c a_s > 0$ holds, the approximated SINR coverage probability of the typical UE $u_0 \in \Phi_U^R$ for the small path loss case is derived as*

$$P_{cov,small}^R(d_{BR,j}^{(i)}, d_{RU,0}^{(i)}) \approx \sum_{n=1}^{m_R} (-1)^{n+1} \binom{m_R}{n} \mathcal{L}_{I_R}(s_R) \mathcal{L}_{I_L}(s_R) \mathcal{L}_{I_N}(s_R) e^{-s_R \sigma^2}, \quad (39)$$

where $s_R = \frac{n\eta_R \tau^*}{P_B L_{RIS}(d_{BR,j}^{(i)}, d_{RU,0}^{(i)})}$. Otherwise, $P_{cov,small}^R(d_{BR,j}^{(i)}, d_{RU,0}^{(i)}) = 0$.

Proof: The proof is similar to the proof in **Lemma 7**. ■

2) *Large Path Loss Case:* In this case, the typical UE decodes its own message by treating the paired connected UE as noise, so the SINR coverage probability is

$$P_{cov,large} = \mathbb{P}(\gamma_{t,large} > \tau_t). \quad (40)$$

Similar to the small path loss case, the conditional SINR coverage probabilities of the typical user for the large path loss case are given in the following propositions.

Proposition 1. *If $a_l - \tau_t a_s > 0$ holds, the approximated SINR coverage probability of the typical UE $u_0 \in \Phi_U^L$ for the large path loss case is derived as*

$$P_{cov,large}^L(d_{0,j}) \approx \sum_{n=1}^{m_L} (-1)^{n+1} \binom{m_L}{n} \mathcal{L}_{I_L}(s_L^l) \mathcal{L}_{I_N}(s_L^l) e^{-s_L^l \sigma^2}, \quad (41)$$

where $s_L^l = \frac{n\eta_L \tau_t^l}{P_{BLBU,L}(d_{0,j})}$ and $\tau_t^l = \frac{\tau_t}{a_l - \tau_t a_s}$. Otherwise, $P_{cov,large}^L(d_{0,j}) = 0$.

Proposition 2. *If $a_l - \tau_t a_s > 0$ holds, the approximated SINR coverage probability of the typical UE $u_0 \in \Phi_U^R$ for the large path loss case is derived as*

$$P_{cov,large}^R(d_{BR,j}^{(i)}, d_{RU,0}^{(i)}) \approx \sum_{n=1}^{m_R} (-1)^{n+1} \binom{m_R}{n} \mathcal{L}_{I_R}(s_R^l) \mathcal{L}_{I_L}(s_R^l) \mathcal{L}_{I_N}(s_R^l) e^{-s_R^l \sigma^2}, \quad (42)$$

where $s_R^l = \frac{n\eta_R \tau_t^l}{P_{BLRIS}(d_{BR,j}^{(i)}, d_{RU,0}^{(i)})}$. Otherwise, $P_{cov,large}^R(d_{BR,j}^{(i)}, d_{RU,0}^{(i)}) = 0$.

Remark 3. *Comparing to the case that the typical UE associates to a LoS BS directly, the typical UE suffers extra interference I_R when associating to a RIS. Thus, when the pass losses for the two kinds of links are similar in value, the typical UE obtains higher SINR from the BS-UE link than the BS-RIS-UE link. In practical application scenarios, we can set a bias factor in the UE association scheme to improve the system performance.*

Now that we have developed expressions of the conditional SINR coverage probability in **Lemma 7-8** and **Proposition 1-2**, the SINR coverage probability of the typical UE can be calculated in the following theorem.

Theorem 2. *For the typical UE in this NOMA RIS HetNets, the SINR coverage probability is expressed as*

$$P_{cov}(\tau_c, \tau_t) = P_{cov}^L(\tau_c, \tau_t) + P_{cov}^R(\tau_c, \tau_t). \quad (43)$$

$P_{cov}^L(\tau_c, \tau_t)$ and $P_{cov}^R(\tau_c, \tau_t)$ are the SINR coverage probabilities when the typical UE is associated with a LoS BS and RIS, respectively, and are given by

$$P_{cov}^L(\tau_c, \tau_t) = \int_0^{d_C} P_{cov,small}^L(x) f_{d_{0,j}}(x) \int_{\varphi^{-1}(x)}^{\infty} f_{d_{0,j}^{(i)}}(y) dy dx + \int_{d_C}^{\infty} P_{cov,large}^L(x) f_{d_{0,j}}(x) \int_{\varphi^{-1}(x)}^{\infty} f_{d_{0,j}^{(i)}}(y) dy dx, \quad (44)$$

$$P_{cov}^R(\tau_c, \tau_t) = \int_0^{\infty} \int_0^{\varphi^{-1}(d_C)/x_1} P_{cov,small}^R(x_1, x_2) \bar{F}_{d_{0,j}}(\varphi(x_1 x_2)) f_{d_{BR}}(x_2) dx_2 f_{d_{RU}}(x_1) dx_1 + \int_0^{\infty} \int_{\varphi^{-1}(d_C)/x_1}^{\infty} P_{cov,large}^R(x_1, x_2) \bar{F}_{d_{0,j}}(\varphi(x_1 x_2)) f_{d_{BR}}(x_2) dx_2 f_{d_{RU}}(x_1) dx_1, \quad (45)$$

where $\varphi^{-1}(x) = (\tilde{c}_{RL})^{\frac{1}{\alpha_R}} x^{\tilde{\alpha}_{LR}}$, and $\bar{F}_{d_{0,j}}(x) = 1 - F_{d_{0,j}}(x)$.

Proof: See Appendix D. ■

Based on the analytical expression of the SINR coverage probability provided in **Theorem 2**, we consider a special case in the RIS HetNets.

Corollary 3. *Conditioned on the half-length of RISs $L \rightarrow \infty$, the asymptotic SINR coverage probability of the typical UE is*

$$P_{cov}(\tau_c, \tau_t) \approx \sum_{n=1}^{m_R} (-1)^{n+1} \binom{m_R}{n} \frac{\lambda_B}{\frac{\tilde{\lambda}_B}{2} Q_R(\eta_R, \tau^*) + \lambda_B}, \quad (46)$$

where $Q_R(\eta, \tau) = {}_2F_1\left(m_R, -\frac{2}{\alpha_R}; 1 - \frac{2}{\alpha_R}; -\frac{n\eta\tau}{m_R}\right) - 1$.

Proof: See Appendix E. ■

Remark 4. *When the length of RISs is sufficiently large, the SINR coverage becomes a constant related to the density of BSs λ_B and the density of active BSs $\tilde{\lambda}_B$. Moreover, if $\lambda_U \gg \lambda_B$, $\tilde{\lambda}_B \rightarrow \lambda_B$ and the SINR coverage $P_{cov}(\tau_c, \tau_t) < 1$. If $\lambda_U \ll \lambda_B$, the density of active BSs $\tilde{\lambda}_B \rightarrow \lambda_U$ and the part $\frac{\tilde{\lambda}_B}{2} Q_R(\eta_R, \tau^*)$ is negligible. In this case, $P_{cov}(\tau_c, \tau_t) \rightarrow 1$. Thus, the enlargement of RISs may not achieve the maximum achievable performance.*

C. Rate Distribution

In this subsection, we evaluate the rate coverage probability of the typical UE. Noticed that the targeted data rate of the connected UE is $\rho_c = B_W \log_2(1 + \gamma_c)$ and that of the typical UE

is $\rho_t = B_W \log_2(1 + \gamma_t)$, where B_W is the available bandwidth, the expression of rate coverage probability can be derived from the SINR coverage probability.

Let N_B denote the number of UEs that associate to a BS. According to [36, Lemma 3], the probability mass function (PMF) of the load at a BS is given by

$$f_B(n) = \mathbb{P}(N_B = n) = \frac{3.5^{3.5} \Gamma(n + 3.5)}{\Gamma(3.5) \Gamma(n)} \left(\frac{\lambda_U}{\lambda_B} \right)^{n-1} \left(3.5 + \frac{\lambda_U}{\lambda_B} \right)^{-(n+3.5)}, \quad (47)$$

where $n \geq 1$ and $\Gamma(\cdot)$ is the gamma function.

Theorem 3. *For the typical UE in the NOMA RIS HetNets, the rate coverage probability is given by*

$$R_{cov}(\rho_c, \rho_t) = \sum_{n \geq 1} f_B(n) \left(P_{cov}^L(\phi(n\rho_c), \phi(n\rho_t)) + P_{cov}^R(\phi(n\rho_c), \phi(n\rho_t)) \right), \quad (48)$$

where $\phi(x) = 2^{x/W} - 1$.

Proof: The probability that the data rate requirement of the typical UE $u_0 \in \Phi_U$ is met is expressed as

$$\begin{aligned} R_{cov}(\tau_c, \tau_t) &= \sum_{T=\{L,R\}} \mathbb{P} \left(\frac{W}{N_B} \log_2(1 + \gamma_t^T) > \rho_t \cap \frac{W}{N_B} \log_2(1 + \gamma_{t \rightarrow c, small}^T) > \rho_c, u_0 \in \Phi_U^T \right) \\ &= \sum_{T=\{L,R\}} \mathbb{P} \left(\gamma_t^T > \phi(\rho_t N_B) \cap \gamma_{t \rightarrow c, small}^T > \phi(\rho_c N_B), u_0 \in \Phi_U^T \right) \\ &= \sum_{T=\{L,R\}} \mathbb{E}_{N_B} \left[P_{cov}^T(\phi(\rho_c N_B), \phi(\rho_t N_B)) \right], \end{aligned} \quad (49)$$

where $\phi(x) = 2^{x/W} - 1$. Using the result in (47), the average value is

$$\mathbb{E}_{N_B} \left[P_{cov}^T(\phi(\rho_c N_B), \phi(\rho_t N_B)) \right] = \sum_{n \geq 1} f_B(n) P_{cov}^T(\phi(n\rho_c), \phi(n\rho_t)). \quad (50)$$

The proof is completed. ■

As shown in (48), the expression of the rate coverage probability includes an infinite summation. For tractability of the analysis, we evaluate the rate coverage by introducing the mean load in the following corollary.

Corollary 4. *The rate coverage probability with the mean load approximation is given by*

$$\bar{R}_{cov}(\rho_c, \rho_t) = P_{cov}^L(\phi(\bar{N}_B \rho_c), \phi(\bar{N}_B \rho_t)) + P_{cov}^R(\phi(\bar{N}_B \rho_c), \phi(\bar{N}_B \rho_t)). \quad (51)$$

Proof: The first moment of load N_B is $\bar{N}_B = \mathbb{E}[N_B] = 1 + \frac{1.28\lambda_U}{\lambda_B}$, [36]. Further, using the approximation $\mathbb{E}_{N_B}[P_{cov}^T(\phi(\rho_c N_B), \phi(\rho_t N_B))] \approx P_{cov}^T(\phi(\rho_c \mathbb{E}[N_B]), \phi(\rho_t \mathbb{E}[N_B]))$, this corollary is proved. ■

Remark 5. *With the growth of λ_U , the load of each BS increases and the available bandwidth for each UE decreases. Hence, the rate coverage probability decreases.*

For the rate coverage, we also consider the special case $L \rightarrow \infty$ in the RIS HetNets.

Corollary 5. *Conditioned on the half-length of RISs $L \rightarrow \infty$, the asymptotic rate coverage probability of the typical UE is*

$$R_{cov}(\tau_c, \tau_t) \approx \sum_{n=1}^{m_R} (-1)^{n+1} \binom{m_R}{n} \frac{\lambda_B}{\frac{\lambda_B}{2} Q_R(\eta_R, \rho^*) + \lambda_B}, \quad (52)$$

where $\rho^* = \max\left(\frac{\phi(\bar{N}_B \rho_c)}{a_l - \phi(\bar{N}_B \rho_c) a_s}, \frac{\phi(\bar{N}_B \rho_t)}{a_s}\right)$.

Proof: The proof is similar to **Corollary 3** and is hence skipped. ■

Remark 6. *Considering the rate coverage probability, the conclusion of RIS enlargement is the same as **Remark 4**.*

V. NUMERICAL RESULTS

In this section, numerical results are presented to validate the UE association and coverage performance of NOMA enhanced RIS HetNets, and then some interesting insights are provided. We assume the network is operated at 28 GHz. The noise power is $\sigma^2 = -170 + 10 \log_{10} W + N_f$. The distance between connected UEs and their BSs is fixed at $d_C = 50$ m. Table II summarizes the simulation parameters used in this section.

A. UE Association Probability

Fig. 2 shows the effect of the density of BSs λ_B and the effect of RISs λ_R on UE association probability. The analytical curves presenting LoS BSs and RISs are from **Theorem 1**, and the bounds P_L and P_N demonstrated in **Remark 1** are validated. One can observe that increasing

TABLE II
TABLE OF PARAMETERS

Bandwidth	$W = 100$ MHz
Path loss exponent	$\alpha_L = 2, \alpha_R = 2.8,$ $\alpha_N = 4$
Nakagami coefficient	$m_L = m_R = 4,$ $m_N = 1$
Power allocation factor	$a_s = 0.3, a_l = 0.7$
Half-length of RIS	$L = 1$ m
Density of UE	$\lambda_U = 100$ km ⁻²
Blockage parameter	$\beta = 1/141.4$
The noise figure	$N_f = 10$ dB
SINR threshold	$\tau_t = \tau_c = -20$ dB
Rate threshold	$\rho_t = \rho_c = 1$ Mbps

the density of RISs encourages more UEs to associate to BSs through BS-RIS-UE links. This is because the RISs are closer to UEs and the reflective signal from RISs suffers smaller path loss than the signal from direct BS-UE links. Another observation is that with the increase of the BS density, the probability that the typical UE directly associates to LoS BSs increases to a maximum first and then keeps steadily. This can be explained that: 1) in sparse scenarios, deploying denser BSs can increase the probability that the BS-UE link exists, and this kind of link brings high received power; 2) in dense scenarios, increasing the density of BSs shortens the distance of both BS-UE links and BS-RIS-UE links, hence the received power from both tiers can be enhanced.

B. SINR Coverage

Verification of the analytical expression of SINR coverage probability (**Theorem 2**) is illustrated in Fig. 3 by sweeping over a range of transmit SNR. The SINR coverage is shown for different densities of BSs and RISs. It is observed that varying the density of BSs brings significant change in SINR coverage performance.

The SINR coverage probability comparison among NOMA RIS HetNets, OMA RIS HetNets and NOMA macro cells scenarios are shown in Fig. 4. We can observe that comparing to macro cells scenarios, introducing the RIS HetNet structure enhances the SINR coverage performance

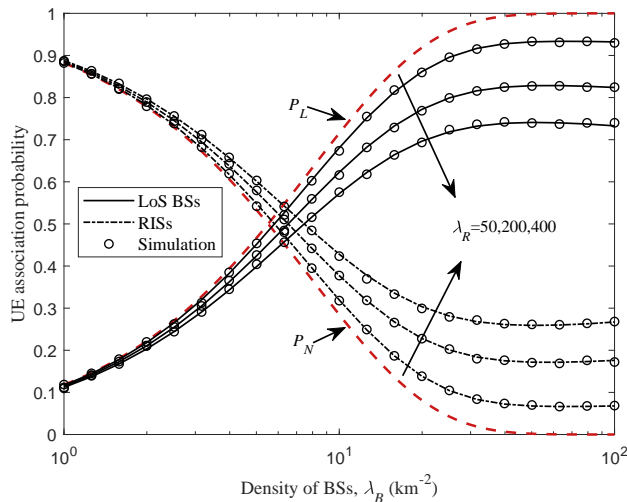


Fig. 2. User association probability versus density of BSs with $\lambda_R = [50, 200, 400] \text{ km}^{-2}$: a verification of **Theorem 1**.

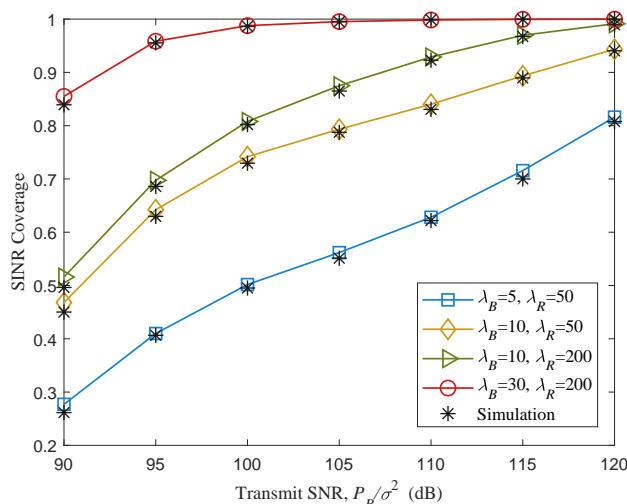


Fig. 3. SINR coverage probability versus transmit SNR with various density of BSs and RISs: a verification of **Theorem 2**.

considerably. This is attributed to the fact that RISs help the blocked UEs associate to NLoS BSs by a LoS reflective transmission path which has much smaller loss. Besides, RISs also supplement SINR coverage of LoS BSs.

Fig. 5 plots the SINR coverage versus the half-length of RISs L for $P_B = 1 \text{ W}$ and $\lambda_B = 10 \text{ km}^{-2}$. We observe that there exists an optimal L to maximize the system performance. For small-sized RISs, increasing the length of RISs improves the SINR coverage probability. This is because that as we increase the length, the channel gain of the BS-RIS-UE link grows and the

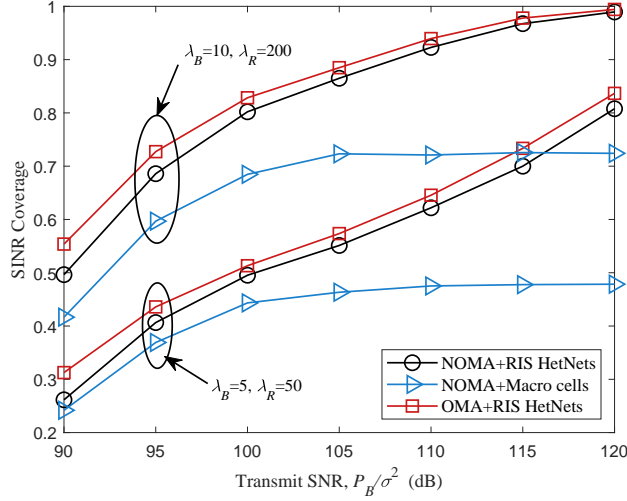


Fig. 4. SINR coverage probability versus transmit SNR: a comparison among NOMA HetNets, OMA RIS HetNets and NOMA Macro cells.

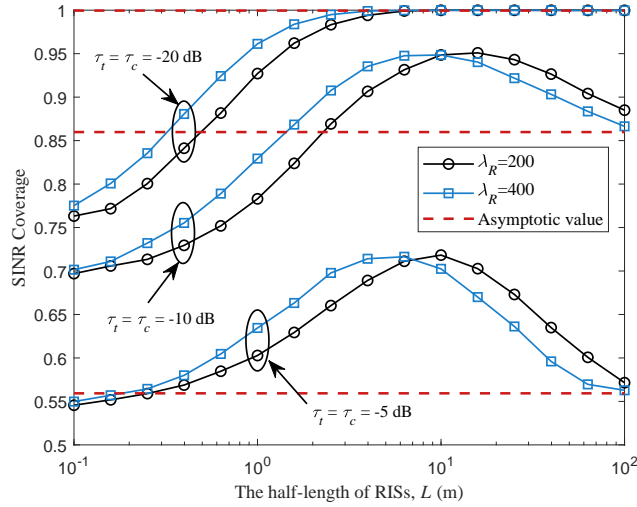


Fig. 5. SINR coverage probability versus half-length of RISs with $\lambda_B = 10 \text{ km}^{-2}$ and $P_B = 1 \text{ W}$.

interference power is dominated by both LoS BSs and RISs. However, with a further increase in the length of RISs, the signal as well as interference power from RISs grows rapidly. More UEs associate to RISs for large received power while these UEs suffer serious interference at the same time, which results in the decrease of SINR coverage. Finally, the value of SINR coverage asymptotically approaches a constant as discussed in **Corollary 3**.

Fig. 6 plots the SINR coverage versus the density of BSs λ_B and the density of RISs λ_R . To observe the trend clearly, we set SINR threshold as $\tau_t = \tau_c = -5 \text{ dB}$. Within the reasonable

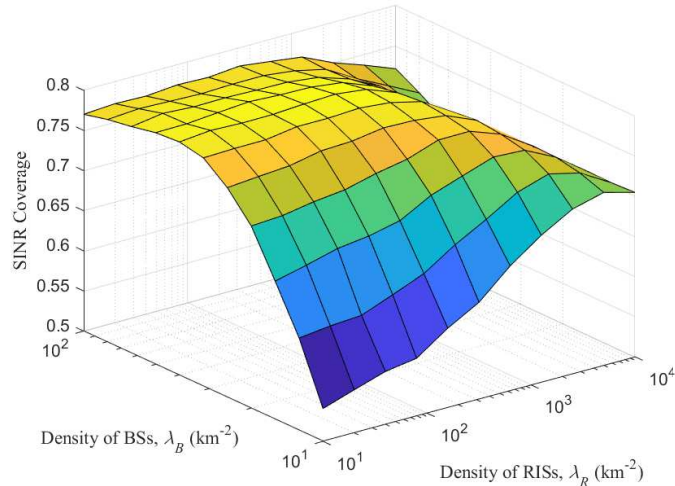


Fig. 6. SINR coverage probability versus density of BSs and density of RISs with $\tau_t = \tau_c = -5$ dB and $P_B = 1$ W.

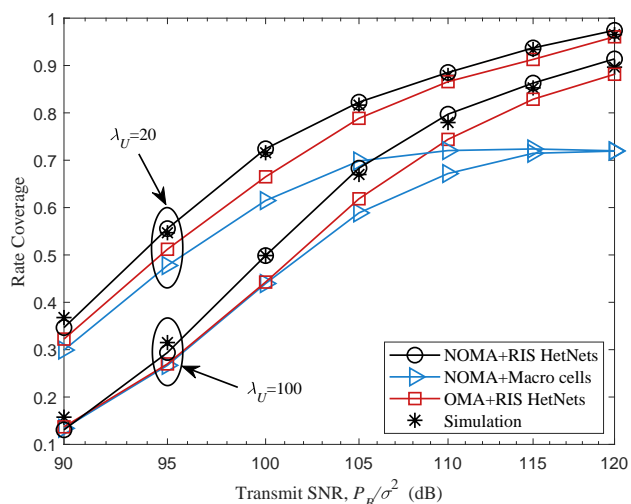


Fig. 7. Rate coverage versus transmit SNR with $\lambda_U = [20, 100]$ km⁻²: a comparison among NOMA HetNets, OMA RIS HetNets and NOMA Macro cells.

range of the parameters, there exists a optimal combination of λ_B and λ_R to maximize the SINR coverage. The reasons are two-fold: 1) similar to the trend of increasing the length of RISs, the SINR coverage decreases finally with the increase of the density of RISs due to the high interference power from RISs; 2) the densification of BSs brings stronger signal power as well as denser LoS interfering BSs.

C. Rate Coverage

In Fig. 7, we compare the rate coverage probability versus transmit SNR for NOMA RIS HetNets, OMA RIS HetNets and NOMA macro cells scenarios. Since the exact expression of the rate coverage in **Theorem 3** is intractable, the curves representing the performance of NOMA RIS HetNets are from **Corollary 4**. It is observed that the rate coverage in NOMA RIS HetNets outperforms the counterpart in other two scenarios. This is because 1) the RIS HetNet structure brings higher channel gain than traditional macro cell networks; 2) the NOMA technique improves bandwidth efficiency. The enhancement of performance validates the effectiveness of our proposed NOMA HetNet framework.

VI. CONCLUSION

In this paper, RIS-aided downlink NOMA networks with a HetNet structure have been investigated, where the stochastic geometry has been utilized for modeling the locations of BSs, RISs, and UEs and evaluating the system performance. A practical UE association scheme has been employed to maximize the average received power. Considering correlated RIS channel, the closed-form PDF of BS-RIS-UE links has been derived, based on which we have presented the UE association probability and its bounds. The analytical expressions of SINR and rate coverage probability have been deduced and validated by numerical results. The coverage enhancement from NOMA schemes and the proposed RIS HetNet structure is verified by comparing to OMA RIS HetNets and NOMA macro cells scenarios. The analysis of this paper has provided guidance for deployment of RISs in the NOMA RIS NetNets: 1) there exists an optimal RIS size for maximum coverage performance; 2) when the density of BSs is known, deploying RISs with an appropriate density can maximize the system coverage.

APPENDIX A: PROOF OF LEMMA 3

As $d_{0,j}^{(i)} = d_{BR,j}^{(i)}d_{RU,0}^{(i)}$, the CDF of $d_{0,j}^{(i)}$ can be given by

$$\begin{aligned}
 F_{d_{0,j}^{(i)}}(z) &= \mathbb{P}(d_{BR,j}^{(i)}d_{RU,0}^{(i)} \leq z) \\
 &= \int_0^\infty \mathbb{P}(d_{BR,j}^{(i)} = x) \mathbb{P}(d_{RU,0}^{(i)} \leq \frac{z}{x}) dx \\
 &= \int_0^\infty f_{d_{BR}}(x) \int_0^{z/x} f_{d_{RU}}(y) dy dx.
 \end{aligned} \tag{A.1}$$

The PDF of $d_{0,j}^{(i)}$ can be obtained from the derivative of $F_{d_{0,j}^{(i)}}(z)$ as

$$f_{d_{0,j}^{(i)}}(z) = \frac{d}{dz} F_{d_{0,j}^{(i)}}(z) = \int_0^\infty \frac{1}{x} f_{d_{BR}}(x) f_{d_{RU}}(z/x) dx. \quad (\text{A.2})$$

By substituting (17) and (18) into (A.2), the PDF of $d_{BU,j}^{(i)}$ can be expressed as

$$\begin{aligned} f_{d_{0,j}^{(i)}}(z) &= 4\pi^2 z \lambda_B \lambda_R \int_0^\infty \frac{1}{x} \exp\left(-\pi \lambda_B x^2 - \pi \lambda_R \frac{z^2}{x^2}\right) dx \\ &\stackrel{(a)}{=} 2\pi^2 z \lambda_B \lambda_R \int_0^\infty \frac{1}{t} \exp\left(-\pi \lambda_B t - \pi \lambda_R \frac{z^2}{t}\right) dt \\ &\stackrel{(b)}{=} 4\pi^2 z \lambda_B \lambda_R K_0\left(2\pi z \sqrt{\lambda_B \lambda_R}\right), \end{aligned} \quad (\text{A.3})$$

where (a) is obtained by employing the change of variable $t = x^2$. (b) is obtained by applying [34, eq. (3.478.4)]. The proof is completed.

APPENDIX B: PROOF OF LEMMA 4

The Laplace transform of the interference from LoS BSs can be expressed as follows

$$\begin{aligned} \mathcal{L}_{I_L}(s) &= \mathbb{E}_{\Phi_B^L} \left[\prod_{k \in \Phi_B^L \setminus j} \mathbb{E}_{h_{0,k}^{L,2}} \left[\exp\left(-s P_B C_L d_{0,k}^{-\alpha_L} h_{0,k}^{L,2}\right) \right] \right] \\ &\stackrel{(a)}{=} \exp\left(-2\pi \tilde{\lambda}_B \int_{d_{0,min}}^\infty \left(1 - \mathbb{E}_{h_{0,k}^{L,2}} \left[\exp\left(-s P_B C_L x^{-\alpha_L} h_{0,k}^{L,2}\right) \right]\right) x p_L(x) dx\right) \\ &\stackrel{(b)}{=} \exp\left(-2\pi \tilde{\lambda}_B \int_{d_{0,min}}^\infty \left(1 - \left(1 + \frac{s P_B C_L}{m_L x^{\alpha_L}}\right)^{-m_L}\right) x p_L(x) dx\right), \end{aligned} \quad (\text{B.1})$$

where (a) follows from probability generating functional (PGFL). (b) is obtained by computing the moment generating function of the gamma random variable $h_{0,k}^{L,2}$.

Then we calculate the minimum interfering distance $d_{0,min}$. If the typical UE associates to a LoS BS, $d_{0,min}^L = d_0$. If the typical UE is aided with a RIS, the nearest interfering LoS BS $k \in \Phi_B^L$ satisfies

$$C_L d_{0,k}^{-\alpha_L} \leq C_R d_{0,j}^{(i)-\alpha_R}. \quad (\text{B.2})$$

Therefore, $d_{0,min}^R = \min d_{0,k} = (\tilde{c}_{LR})^{\frac{1}{\alpha_L}} d_{0,j}^{(i)\frac{\alpha_{RL}}{\alpha_L}}$. According to the maximum average received power association scheme applied in this work, $d_{0,min} = \min\{d_{0,min}^L, d_{0,min}^R\}$. This lemma is proved.

APPENDIX C: PROOF OF LEMMA 6

The Laplace transform of the interference from RISs can be expressed as

$$\begin{aligned}
\mathcal{L}_{I_R}(s) &= \mathbb{E}_{\Phi_B^R} \left[\prod_{k \in \Phi_B^R \setminus j} \mathbb{E}_{h_{0,k}^R} \left[\exp \left(-s P_B C_R \left(d_{BR,k}^{(i)} d_{RU,0}^{(i)} \right)^{-\alpha_R} h_{0,k}^R \right) \right] \right] \\
&\stackrel{(a)}{=} \exp \left(-\pi \tilde{\lambda}_B \int_{d_{BR,j}^{(i)}}^{\infty} \left(1 - \mathbb{E}_{h_{0,j}^R} \left[\exp \left(-s P_B C_R x^{-\alpha_R} d_{RU,0}^{(i)} h_{0,k}^R \right) \right] \right) x dx \right) \\
&= \exp \left(-\pi \tilde{\lambda}_B \int_{d_{BR,j}^{(i)}}^{\infty} \left(1 - \left(1 + \frac{s P_B C_R}{m_R \left(d_{RU,0}^{(i)} x \right)^{\alpha_R}} \right)^{-m_R} \right) x dx \right), \tag{C.1}
\end{aligned}$$

where (a) follows the fact that BSs located at the back of the RIS would not become the interfering BSs.

We denote $A = \frac{s P_B C_R}{m_R d_{RU,0}^{\alpha_R}}$, $B = d_{BR,j}^{(i)}$, and $C = \pi \tilde{\lambda}_B$ for simplicity. The Laplace transform can be rewritten as

$$\begin{aligned}
\mathcal{L}_{I_R}(s) &= \exp \left(-C \int_B^{\infty} \left(1 - \left(1 + A x^{-\alpha_R} \right)^{-m_R} \right) x dx \right) \\
&\stackrel{(b)}{=} \exp \left(\frac{C}{\alpha_R A} \int_0^{-AB^{-\alpha_R}} \left(1 - (1-t)^{-m_R} \right) \left(-\frac{t}{A} \right)^{-2/\alpha_R - 1} dx \right) \\
&\stackrel{(c)}{=} \exp \left(\frac{CB^2}{2} - \frac{CB^2}{2} {}_2F_1 \left(m_R, -\frac{2}{\alpha_R}; 1 - \frac{2}{\alpha_R}; -AB^{-\alpha_R} \right) \right) \tag{C.2}
\end{aligned}$$

where (b) is obtained by employing the change of variable $t = -Ax^{-\alpha_R}$. (c) is obtained by applying [34, eq. 8.391]. The proof is completed.

APPENDIX D: PROOF OF THEOREM 2

Since there are two kinds of links for the typical UE to associates to a BS, let $T = \{L, R\}$ denote the association choice of the typical UE, the probability that the SINR requirement of a random UE $u_0 \in \Phi_U$ is met is

$$P_{cov}(\tau_c, \tau_t) = \sum_{T=\{L,R\}} P_{cov}^T(\tau_c, \tau_t) = \sum_{T=\{L,R\}} \mathbb{P}(\gamma_t^T > \tau_t \cap \gamma_{t \rightarrow c, small}^T > \tau_c, u_0 \in \Phi_U^T). \tag{D.1}$$

For the case that the typical UE associates to a LoS BS directly, $P_{0,j} > P_{0,j}^{(i)}$ holds, so we have $d_{BR,j}^{(i)} d_{RU,0}^{(i)} > \varphi^{-1}(d_{0,j})$, where $\varphi^{-1}(x) = (\tilde{c}_{RL})^{\frac{1}{\alpha_R}} x^{\tilde{\alpha}_{LR}}$. The SINR coverage probability can be

expressed as

$$\begin{aligned}
P_{cov}^L(\tau_c, \tau_t) &= \int_0^{d_C} \int_{\varphi^{-1}(x)}^{\infty} P_{cov,small}^L(x) f_{d_{0,j}}(x) f_{d_{0,j}^{(i)}}(y) dy dx \\
&+ \int_{d_C}^{\infty} \int_{\varphi^{-1}(x)}^{\infty} P_{cov,large}^L(x) f_{d_{0,j}}(x) f_{d_{0,j}^{(i)}}(y) dy dx.
\end{aligned} \tag{D.2}$$

For the case that the typical UE associates to a RIS, the association condition can be rewritten as $d_{0,j} > \varphi(d_{BR,j}^{(i)} d_{RU,0}^{(i)})$, so the SINR coverage probability can be expressed as

$$\begin{aligned}
P_{cov}^R(\tau_c, \tau_t) &= \int_0^{\infty} \int_0^{\zeta(d_C)/x_1} \int_{\varphi(x_1 x_2)}^{\infty} P_{cov,small}^R(x_1, x_2) f_{d_{0,j}}(x_3) dx_3 f_{d_{BR}}(x_2) dx_2 f_{d_{RU}}(x_1) dx_1 \\
&+ \int_0^{\infty} \int_{\zeta(d_C)/x_1}^{\infty} \int_{\varphi(x_1 x_2)}^{\infty} P_{cov,large}^R(x_1, x_2) f_{d_{0,j}}(x_3) dx_3 f_{d_{BR}}(x_2) dx_2 f_{d_{RU}}(x_1) dx_1.
\end{aligned} \tag{D.3}$$

Noticed that the integral $\int_A^{\infty} f_{d_{0,j}}(x) dx = 1 - F_{d_{0,j}}(A) = \bar{F}_{d_{0,j}}(A)$, (45) is obtained. The proof is completed.

APPENDIX E: PROOF OF COROLLARY 3

When $L \rightarrow \infty$, the intercept $C_R \rightarrow \infty$, hence the path loss for the BS-RIS-UE link is always smaller than the BS-UE link. Therefore, the typical UE always associates to the RIS, i.e. $A_R = 1$ holds. In this case, the SINR coverage probability for the typical UE is rewritten as $P_{cov}(\tau_c, \tau_t) = P_{cov}^R(\tau_c, \tau_t)$. Besides, for a finite value x , $\varphi(x) \rightarrow 0$ holds. The SINR coverage can be expressed as

$$\begin{aligned}
P_{cov}(\tau_c, \tau_t) &= \int_0^{\infty} \int_0^{\zeta(d_C)/x_1} P_{cov,small}^R(x_1, x_2) f_{d_{BR}}(x_2) dx_2 f_{d_{RU}}(x_1) dx_1 \\
&+ \int_0^{\infty} \int_{\zeta(d_C)/x_1}^{\infty} P_{cov,large}^R(x_1, x_2) f_{d_{BR}}(x_2) dx_2 f_{d_{RU}}(x_1) dx_1 \\
&\stackrel{(a)}{=} \int_0^{\infty} \int_0^{\infty} P_{cov,small}^R(x_1, x_2) f_{d_{BR}}(x_2) dx_2 f_{d_{RU}}(x_1) dx_1 \\
&\stackrel{(b)}{\approx} \int_0^{\infty} \int_0^{\infty} \sum_{n=1}^{m_R} (-1)^{n+1} \binom{m_R}{n} \mathcal{L}_{I_R}(s_R) f_{d_{BR}}(x_2) dx_2 f_{d_{RU}}(x_1) dx_1 \\
&= 2\pi\lambda_B \sum_{n=1}^{m_R} (-1)^{n+1} \binom{m_R}{n} \int_0^{\infty} x_2 \exp\left(-\pi\left(\tilde{\lambda}_B A + \lambda_B\right)x_2^2\right) dx_2 \\
&= \sum_{n=1}^{m_R} (-1)^{n+1} \binom{m_R}{n} \frac{\lambda_B}{\tilde{\lambda}_B A + \lambda_B},
\end{aligned} \tag{E.1}$$

where $A = \frac{1}{2}Q_R(\eta_R, \tau^*)$ and $Q_R(\eta, \tau) = {}_2F_1\left(m_R, -\frac{2}{\alpha_R}; 1 - \frac{2}{\alpha_R}; -\frac{n\eta\tau}{m_R}\right) - 1$. (a) is resulted from $\zeta(d_C) \rightarrow \infty$. (b) is obtained by using the fact that the interference power from RISs dominates the aggregate interference and the noise power is negligible when $L \rightarrow \infty$. The proof is completed.

REFERENCES

- [1] Z. Xie, W. Yi, X. Wu, Y. Liu, and A. Nallanathan, "Coverage analysis for RIS-aided NOMA heterogeneous networks," in *IEEE Proc. of Global Commun. Conf. (GLOBECOM)*, Dec. submitted.
- [2] Y. Liu, X. Liu, X. Mu, T. Hou, J. Xu, Z. Qin, M. Di Renzo, and N. Al-Dhahir, "Reconfigurable Intelligent Surfaces: Principles and Opportunities," *arXiv e-prints*, p. arXiv:2007.03435, Jul. 2020.
- [3] Q. Wu, S. Zhang, B. Zheng, C. You, and R. Zhang, "Intelligent reflecting surface aided wireless communications: A tutorial," *IEEE Trans. Commun.*, pp. 1–1, 2021.
- [4] C. Huang, A. Zappone, G. C. Alexandropoulos, M. Debbah, and C. Yuen, "Reconfigurable intelligent surfaces for energy efficiency in wireless communication," *IEEE Trans. Wireless Commun.*, vol. 18, no. 8, pp. 4157–4170, 2019.
- [5] W. Tang, J. Y. Dai, M. Z. Chen, K. K. Wong, X. Li, X. Zhao, S. Jin, Q. Cheng, and T. J. Cui, "MIMO transmission through reconfigurable intelligent surface: System design, analysis, and implementation," *IEEE J. Sel. Areas Commun.*, vol. 38, no. 11, pp. 2683–2699, 2020.
- [6] M. Di Renzo, A. Zappone, M. Debbah, M. S. Alouini, C. Yuen, J. de Rosny, and S. Tretyakov, "Smart radio environments empowered by reconfigurable intelligent surfaces: How it works, state of research, and the road ahead," *IEEE J. Sel. Areas Commun.*, vol. 38, no. 11, pp. 2450–2525, 2020.
- [7] M. Di Renzo, K. Ntontin, J. Song, F. H. Danufane, X. Qian, F. Lazarakis, J. De Rosny, D. T. Phan-Huy, O. Simeone, R. Zhang, M. Debbah, G. Lerosey, M. Fink, S. Tretyakov, and S. Shamai, "Reconfigurable intelligent surfaces vs. relaying: Differences, similarities, and performance comparison," *IEEE Open J. Commun. Soc.*, vol. 1, pp. 798–807, 2020.
- [8] M. A. Kishk and M. S. Alouini, "Exploiting randomly located blockages for large-scale deployment of intelligent surfaces," *IEEE J. Sel. Areas Commun.*, vol. 39, no. 4, pp. 1043–1056, 2021.
- [9] Z. Ding, Z. Yang, P. Fan, and H. V. Poor, "On the performance of non-orthogonal multiple access in 5G systems with randomly deployed users," *IEEE Signal Process. Lett.*, vol. 21, no. 12, pp. 1501–1505, 2014.
- [10] L. Dai, B. Wang, Y. Yuan, S. Han, I. Chih-lin, and Z. Wang, "Non-orthogonal multiple access for 5G: solutions, challenges, opportunities, and future research trends," *IEEE Commun. Mag.*, vol. 53, no. 9, pp. 74–81, 2015.
- [11] S. M. R. Islam, N. Avazov, O. A. Dobre, and K. Kwak, "Power-domain non-orthogonal multiple access (NOMA) in 5G systems: Potentials and challenges," *IEEE Commun. Surv. Tuts.*, vol. 19, no. 2, pp. 721–742, 2017.
- [12] A. S. d. Sena, D. Carrillo, F. Fang, P. H. J. Nardelli, D. B. d. Costa, U. S. Dias, Z. Ding, C. B. Papadias, and W. Saad, "What role do intelligent reflecting surfaces play in multi-antenna non-orthogonal multiple access?" *IEEE Wireless Commun.*, vol. 27, no. 5, pp. 24–31, 2020.
- [13] C. Zhang, W. Yi, and Y. Liu, "Reconfigurable Intelligent Surfaces Aided Multi-Cell NOMA Networks: A Stochastic Geometry Model," *arXiv e-prints*, p. arXiv:2008.08457, Aug. 2020.
- [14] I. Yildirim, A. Uyrus, and E. Basar, "Modeling and analysis of reconfigurable intelligent surfaces for indoor and outdoor applications in future wireless networks," *IEEE Trans. Commun.*, vol. 69, no. 2, pp. 1290–1301, 2021.
- [15] Y. Yang, B. Zheng, S. Zhang, and R. Zhang, "Intelligent reflecting surface meets OFDM: Protocol design and rate maximization," *IEEE Trans. Commun.*, vol. 68, no. 7, pp. 4522–4535, 2020.
- [16] Z. Wan, Z. Gao, F. Gao, M. Di Renzo, and M. S. Alouini, "Terahertz massive MIMO with holographic reconfigurable intelligent surfaces," *IEEE Trans. Commun.*, pp. 1–1, 2021.

- [17] H. Hashida, Y. Kawamoto, and N. Kato, "Intelligent reflecting surface placement optimization in air-ground communication networks toward 6G," *IEEE Wireless Commun.*, vol. 27, no. 6, pp. 146–151, 2020.
- [18] J. Lyu and R. Zhang, "Spatial throughput characterization for intelligent reflecting surface aided multiuser system," *IEEE Wireless Commun. Lett.*, vol. 9, no. 6, pp. 834–838, 2020.
- [19] Y. Zhu, G. Zheng, and K. K. Wong, "Stochastic geometry analysis of large intelligent surface-assisted millimeter wave networks," *IEEE J. Sel. Areas Commun.*, vol. 38, no. 8, pp. 1749–1762, 2020.
- [20] J. Lyu and R. Zhang, "Hybrid Active/Passive Wireless Network Aided by Intelligent Reflecting Surface: System Modeling and Performance Analysis," *arXiv e-prints*, p. arXiv:2004.13318, Apr. 2020.
- [21] Z. Ding and H. Vincent Poor, "A simple design of IRS-NOMA transmission," *IEEE Commun. Lett.*, vol. 24, no. 5, pp. 1119–1123, 2020.
- [22] F. Fang, Y. Xu, Q. V. Pham, and Z. Ding, "Energy-efficient design of IRS-NOMA networks," *IEEE Trans. Veh. Technol.*, vol. 69, no. 11, pp. 14 088–14 092, 2020.
- [23] M. Fu, Y. Zhou, Y. Shi, and K. B. Letaief, "Reconfigurable intelligent surface empowered downlink non-orthogonal multiple access," *IEEE Trans. Commun.*, pp. 1–1, 2021.
- [24] J. Zuo, Y. Liu, Z. Qin, and N. Al-Dhahir, "Resource allocation in intelligent reflecting surface assisted NOMA systems," *IEEE Trans. Commun.*, vol. 68, no. 11, pp. 7170–7183, 2020.
- [25] W. Ni, X. Liu, Y. Liu, H. Tian, and Y. Chen, "Resource allocation for multi-cell IRS-aided NOMA networks," *IEEE Trans. Wireless Commun.*, pp. 1–1, 2021.
- [26] Y. Cheng, K. H. Li, Y. Liu, K. C. Teh, and H. Vincent Poor, "Downlink and uplink intelligent reflecting surface aided networks: NOMA and OMA," *IEEE Trans. Wireless Commun.*, pp. 1–1, 2021.
- [27] T. Hou, Y. Liu, Z. Song, X. Sun, Y. Chen, and L. Hanzo, "Reconfigurable intelligent surface aided NOMA networks," *IEEE J. Sel. Areas Commun.*, vol. 38, no. 11, pp. 2575–2588, 2020.
- [28] —, "MIMO Assisted Networks Relying on Intelligent Reflective Surfaces," *arXiv e-prints*, p. arXiv:1910.00959, Oct. 2019.
- [29] S. Lee and K. Huang, "Coverage and economy of cellular networks with many base stations," *IEEE Commun. Lett.*, vol. 16, no. 7, pp. 1038–1040, 2012.
- [30] M. Di Renzo, F. Habibi Danufane, X. Xi, J. de Rosny, and S. Tretjakov, "Analytical modeling of the path-loss for reconfigurable intelligent surfaces - anomalous mirror or scatterer ?" in *Proc. IEEE 21th Int. Workshop Signal Process. Adv. Wireless Commun. (SPAWC)*, 2020, pp. 1–5.
- [31] T. Bai and R. W. Heath, "Coverage and rate analysis for millimeter-wave cellular networks," *IEEE Trans. Wireless Commun.*, vol. 14, no. 2, pp. 1100–1114, 2015.
- [32] M. Haenggi, *Stochastic Geometry for Wireless Networks*. New York, USA: Cambridge University Press, 2013.
- [33] T. Bai, R. Vaze, and R. W. Heath, "Analysis of blockage effects on urban cellular networks," *IEEE Trans. Wireless Commun.*, vol. 13, no. 9, pp. 5070–5083, 2014.
- [34] I. Gradshteyn and I. Ryzhik, *Table of Integrals, Series, and Products*, 7th ed. Boston, USA: Academic Press, 2007.
- [35] H. Alzer, "On some inequalities for the incomplete gamma function," *Math. Comput.*, vol. 66, no. 218, pp. 771–778, 1997.
- [36] S. Singh and J. G. Andrews, "Joint resource partitioning and offloading in heterogeneous cellular networks," *IEEE Trans. Wireless Commun.*, vol. 13, no. 2, pp. 888–901, 2014.